AIAA SciTech Forum
8–12 January 2018, Kissimmee, Florida
2018 AIAA Aerospace Sciences Meeting

10.2514/6.2018-2255

Pulse Actuation and Its Effects on Separated Lagrangian Coherent Structures for Flow over a Cambered Airfoil

Martin H. Kamphuis* and Gustaaf B. Jacobs†*
Department of Aerospace Engineering
San Diego State University
San Diego, CA 92182-1308

Kevin K. Chen ‡
Center for Communications Research
Institute of Defense Analysis - La Jolla
San Diego, CA 92121

Geoffrey Spedding §
Department of Aerospace Engineering
University of Southern California
Los Angeles, CA 90089-1453

Harry W. M. Hoeijmakers¶
Department of Eng. Fluid Dynamics
Universiteit Twente
Enschede, The Netherlands, 7500 AE

The effects of a pulse actuation on the Lagrangian Coherent Structures (LCS) in the separated flow over a NACA 65(1)-412 airfoil at low Reynolds number is investigated. A computational parametric study is performed on the effect of location over the suction side of the airfoil. An increased local separation angle leads to flow reattachment of the Lagrangian material line. Reattachment is accompanied by an increase in the lift and reduction in drag. The optimal pulse actuation is near the Lagrangian separation point.

INTRODUCTION

The efficiency and the performance of turbomachinery is largely influenced by the lift and drag polars of a compressor or turbine blade. At high angles of attack flow separation yields a sharp decrease in lift and an increase in drag. The accompanying total pressure losses deteriorate the performance of the machine.

Much effort has gone towards control of the airfoil aerodynamics to prevent this performance loss (See textbooks like 1,2 for discussion on blowing, suction and other control techniques). Recent control strategies have focused on synthetic jets,[3,4] plasma actuators,[5] and acoustic streaming.[6] These control methods have in common that they attempt to obtain significant performance improvement without complex mechanical actuation, use of external pumps or changes in the airfoil geometry. Synthetic jets, for example, can be integrated into the airfoil and do not require an external air supply, i.e. a synthetic jet has zero-net mass flux. The placement of control devices depends strongly on parameters such as the location of the separation point, airfoil geometry, free-stream conditions, etc. Most studies performed place the controller at an intuitively optimal location. In 3 and 7, for example, the effects of the synthetic jet placed near the trailing edge was investigated to emulate a Gurney flap. While intuitively, it makes sense to place the controller near the

*Student
†Professor, Associate Fellow AIAA, Corresponding Author: gjacobs@mail.sdsu.edu.
‡Staff Scientist.
§Professor, Associate Fellow AIAA.
¶Professor, Associate Fellow AIAA.

separation point and/or to manipulate the Kutta condition, Chen[8] shows that the optimal placement of a controller in general is not trivial.

Optimal placement, for example, requires a detailed understanding of non-linear flow phenomena like flow separation and non-linear flow feedback of the wake. Commonly, in two dimensions, seperation locations are identified by the location of zero skin friction on the airfoil surface. In Haller,[9] however, it was shown that an unsteady flow separation is better analyzed in the Lagrangian frame. The separation line combined with the so-called Lagrangian Coherent Structures (LCS)[10] form a set of material lines that determine the dynamics and hence lift and drag of the airfoil.

In this paper, we investigate the sensitivity of the Lagrangian separation and connected separation line subject to pulse actuation in the boundary layer. The lessons learned from pulse actuation provide the basis for the determination of the optimal placement of actuators[11] and associated development of an active feedback control. The location of the pulse and its flow response are used to investigate the sensivity of LCS to a flow control device.

A NACA 65(1)-412 airfoil (Fig. 1) is considered because it is representative for a compressor blade airfoil, our focus application. Two-dimensional Direct Numerical Simulations (DNS) are performed at moderate Reynolds numbers and at design angles of attack. It is shown that pulse actuation near the separation point, can increase the instantaneous lift coefficient up to 40%. This increase is accompanied by significant flow reattachment.

In the next section, we summarize the numerical method, followed by a summary of the Lagrangian theory. Subsequently, results of the effects of pulsed actuation on the separated flow over the airfoil are discussed. Conclusions are reserved for the last section.

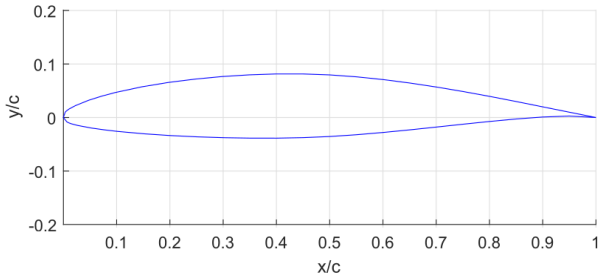

Figure 1. NACA 65(1)-412 AIRFOIL

METHODOLOGY

Governing Equations

We consider the Navier-Stokes equations for two-dimensional flows in conservation form

$$\begin{aligned} \frac{\partial \rho}{\partial t} + \nabla \cdot (\rho \mathbf{u}) &= 0, \\ \frac{\partial (\rho \mathbf{u})}{\partial t} + \nabla \cdot (\rho \mathbf{u} \otimes \mathbf{u} + p\mathbf{I} - \tau) &= \mathbf{M}, \\ \frac{\partial (\rho E)}{\partial t} + \nabla \cdot (\rho E \mathbf{u} + p\mathbf{u} - \tau \cdot \mathbf{u} - k\nabla T) &= \mathbf{u} \cdot \mathbf{M}, \end{aligned} \tag{1}$$

where ρ is the density, u and v the velocity in x- and y-direction resspectibely, p the pressure, T the temperature, and E is the total energy. k is the conductivity of the fluid and τ is the viscous stress tensor. $\mathbf{M}$ represents the momentum source that later in the paper models the pulse. A zero-net mass flux source is considered and hence the source term in the continuity equation is absent. An in-house DNS solver based on a Discontinuous Galerkin-Spectral Element Method that was extensively tested for numerical simulation of the flow around the airfoil[12] is used to numerically solve the governing equations.

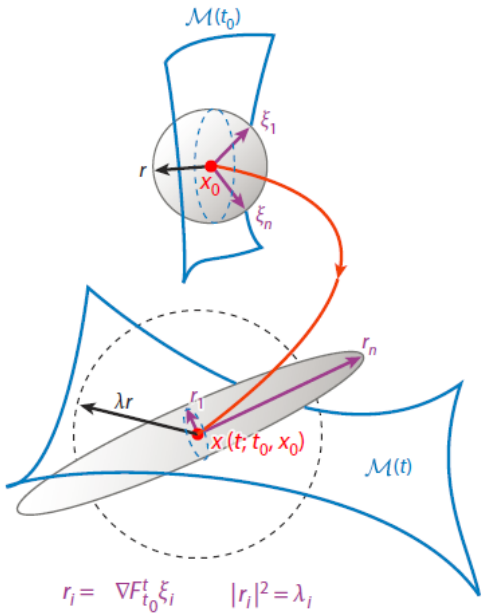

Figure 2. DEFORMATION OF A SPHERICAL FLUID ELEMENT, THE FTLE IS DETERMINED BY THE LARGEST EIGENVALUE OF THE DEFORMATION GRADIENT[10]

Lagrangian Coherent Structures

We investigate the effect of a pulse on the Lagrangian dynamics of the flow as described by LCS theory.[10] LCS may be visualized using the Finite-Time Lyapunov Exponent (FTLE), which determines the maximum stretching of a finite blob of fluid as it is advected over a finite time (Fig. 2). The FTLE is computed numerically according to the algorithm presented in 13 and is based on the determination of a finite time flow map as follows:

$$\phi_{t_0}^{t_1}(\mathbf{x}_0) = \mathbf{x}\left(\mathbf{x}_0, t_0, t_1\right) = \mathbf{x}_0 + \int_{t_0}^{t_1} \mathbf{u}\left(\mathbf{x}(s), s\right)\, ds, \tag{2}$$

The deformation gradient of the flow map is related to the strain field through the Cauchy-Green strain tensor, which is defined as

$$\mathbf{C}_{t_0}^{t_1}(\mathbf{x}_0) = \left(\phi_{t_0}^{t_1}(\mathbf{x}_0)\right)^T \phi_{t_0}^{t_1}(\mathbf{x}_0). \tag{3}$$

The FTLE is the maximum eigenvalue of the Cauchy-Green tensor and represents the maximum deformation of the fluid element over a time interval. FTLEs can either be repelling or attracting depending on whether the flow map is traced forward or backward in time. Maxima in the FTLE field identify material lines that separate fluid. Along attracting (stable) material lines, fluid particles are stretched tangentially whereas for repelling (unstable) material lines, the fluid is stretched normal to the material line (Fig. 3). The attractor is closely related to separation while the repeller is closely connected to reattachment.[14]

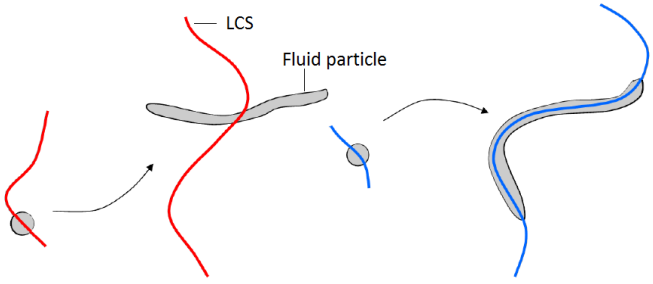

Figure 3. ILLUSTRATION OF REPELLING LCS (LEFT), GIVEN BY FORWARD-TIME FTLE, AND ATTRACTING LCS (RIGHT), GIVEN BY BACKWARD-TIME FTLE[13]

Flow Separation in the Lagrangian Frame

A separated material line has characteristics that are very similar to an attracting LCS.[10] Both lines collect and stretch fluid along their path. However, since the velocity at a no-slip wall is equal to zero, the line close to a surface cannot be a repeller or an attractor (no material is attracted or repelled at the zero velocity wall location). Hence the maximum FTLE line can not be an identifier of the separation line near the wall and a different approach is required.

Using a non-linear dynamical systems approach, Haller[9] derived a formula for to the separation line based on the continuity equation and the no-slip condition. He found that for flows with an asymptotic mean, the separation point γ is located at the location of zero time-averaged skin friction

$$\frac{1}{t_1-t_0}\int_{t_0}^{t_1} c_f(\gamma,t)\,dt = 0. \tag{4}$$

The separation angle as a function of time is determined from the pressure and skin-friction at the separation location as

$$\tan(\theta(t_0)) = \frac{\lim_{T\to-\infty} -3\frac{1}{T}\int_{t_0}^{T}\tau_x(\gamma,t)dt}{\lim_{T\to-\infty}\frac{1}{T}\int_{t_0}^{T}\left[p_x(\gamma,y_w,t)+3\tau_x(\gamma,t)\int_{t_0}^{t}\frac{1}{\mu}\tau(\gamma,s)ds\right]dt}. \tag{5}$$

From the separation angle $\theta(t_0)$ and the separation location γ, a linear approximation of the separation line can be constructed. Since this separation line divides fluid material, just like an LCS, eventually it can be expected to coincide with a stable manifold. To the best of our knowledge this intersection has not yet been reported in literature.

Numerical Method

To test the effect of a pulse control on the separated flow over an airfoil, the NACA 65(1)-412 airfoil is considered at an angle of attack of, α=4°. The airfoil geometry is representative of that of a compressor blade. The angle of attack is typical for a design condition of a compressor. We take a low-speed free-stream Mach number of Ma_∞=0.3, which ensures that firstly compressibility effects are small and secondly that the explicit time integration step is not restrictive on computational cost for the simulation. A moderate Reynolds number of Re_c=20,000 yields unsteady flow structures which we intend to control and ensures computational feasibility of the use of the DNS method.

The computational domain and grid are shown in Figure 4. Inflow and outflow boundary conditions are applied at the boundaries of the computational domain, and the wall boundary condition is no-slip. The grid comprises of 2256 elements. With a twelfth-order basis it was shown in 12 that the simulation is grid-converged.

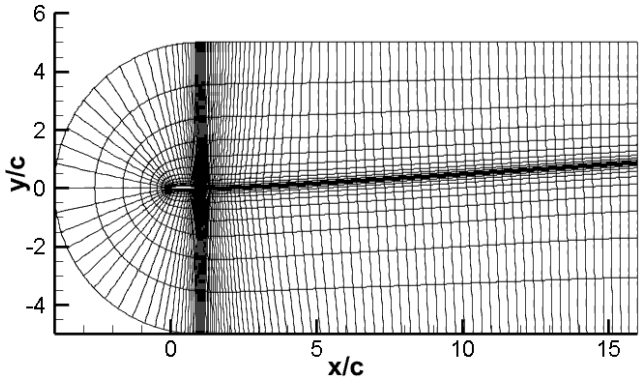

Figure 4. COMPUTATIONAL GRID USED FOR THE SIMULATIONS FOR THE FLOW AROUND A NACA 65(1)-412 AIRFOIL AT $\alpha = 4°$, $Re_c = 20,000$

A parametric study is conducted on the effect of the pulse location. A pulse actuation is applied at the suction side of the airfoil, at each tenth of a chord line, between $x/c = 0.1$ and $x/c = 0.6$. A case without pulse actuation is also considered to serve as a reference (referred to "baseline" case hereafter).

The pulse actuation is applied when the baseline flow is periodic and a vortex street has formed in the airfoil's wake (Fig. 5). The flow is determined to be quasi-periodic after ten convective time units, t =10, when the lift coefficient and the drag coefficient are periodically changing in time and have an evident mean value.

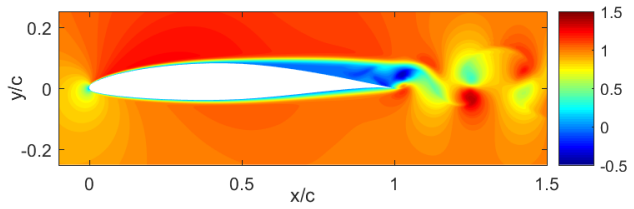

Figure 5. NACA 65(1)-412, $\alpha = 4°$, $Re_c = 20,000$, CONTOURS AT $t = 10$ OF THE QUASI-STEADY u-VELOCITY FIELD

Modeling of the Pulse

The pulse force is modeled by distributing a body force field

$$\mathbf{F}_{pulse} = \int_{\Omega_{jet}} \mathbf{M_s}\left(\mathbf{x}, t\right)\, d\Omega_{jet}. \tag{6}$$

over the area Ω_{jet} as described in 15, 16.

A two-dimensional Gaussian function is used to distribute this force leading to

$$\mathbf{M_s}(x_1, y_1, t) = \frac{\mathbf{F}_{pulse}}{2\pi\sigma_{x_1}\sigma_{y_1}} \exp\left(-\frac{(x_1 - x_c)^2}{2\sigma_{x_1}^2} - \frac{(y_1 - y_c)^2}{2\sigma_{y_1}^2}\right). \tag{7}$$

where x_c and y_c identify the location of the pulse and σ_{x_1} and σ_{y_1} represents the support of the Gaussian distribution function. For the support, a scaling of $\sigma_{x_1}/0.12c = 0.01$ and $\sigma_{y_1}/0.12c = 0.08$ is used.[15] To determine the magnitude of the force, we consider an equivalent pulsed jet flow through through a surface with area A_{jet} with a velocity $\mathbf{u}_{jet}$ as

$$\mathbf{F}_{pulse} = \rho|\mathbf{u}_{jet}(t)|\mathbf{u}_{jet}(t)A_{jet}. \tag{8}$$

A pulse actuation affects the spatially distributed forcing through a Dirac delta function in time as follows

$$\mathbf{M}(\mathbf{x}, t) = \mathbf{M_s}(\mathbf{x})\delta(t). \tag{9}$$

Integration of this source leads to a single contribution at the time of the pulse. To numerically model the pulse one therefore only requires to add the integrated force distribution to the time of pulse as

$$\mathbf{Q}(\mathbf{x}, 0^+) = \mathbf{Q}(\mathbf{x}, 0^-) + \mathbf{M_s}(\mathbf{x}), \tag{10}$$

where $\mathbf{Q}(\mathbf{x}, 0^+)$ and $\mathbf{Q}(\mathbf{x}, 0^-)$ represent the solution vector $[\rho\ \ \rho u\ \ \rho v\ \ \rho E]^T$ right before and right after the pulse, respectively. The pulse is applied at the initial time, t=10, and is actuated normal to the separated shear layer that develops on the suction side of the airfoil. The pulse strength is determined with $\mathbf{u}_{jet}$=1.68 U_∞ and A_{jet}=0.05c.

RESULTS AND DISCUSSION

Baseline Flow

From the time sequence of the attracting LCS' for the baseline case in Figures 6a-d, a periodic vortex shedding and corresponding asymmetric vortex street in the airfoil's wake is observed. The separation LCS on the suction side that coincides with the separated shear layer (not shown here) separates the outer flow from a recirculating flow between the separation line and the airfoil's surface.

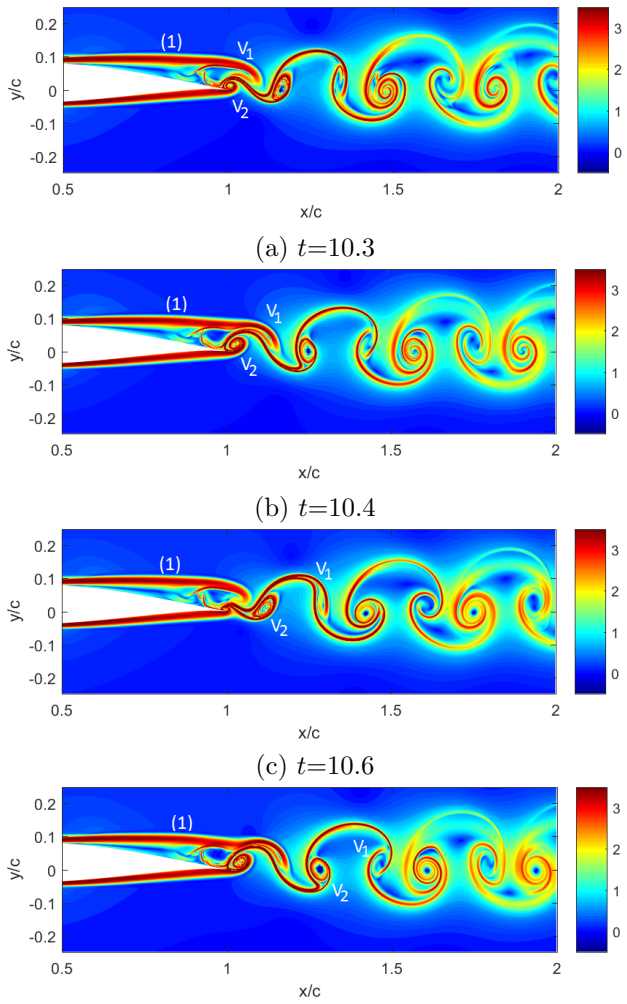

(a) t=10.3

(b) t=10.4

(c) t=10.6

(d) t=10.8

Figure 6. NACA 65(1)-412, $\alpha = 4°$, $Re_c = 20,000$, BACKWARD-TIME FTLE FIELD NEAR THE WAKE AT (a) t= 10.30, (b) t=10.4, (c) t=10.6, and (d) t=10.8 FOR THE BASELINE CASE (NO PULSE ACTUATION)

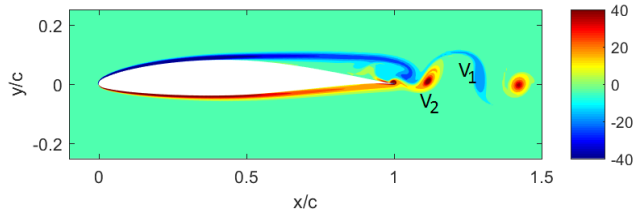

Figure 7. NACA 65(1)-412, $\alpha = 4°$, $Re_c = 20,000$, VORTICITY FIELD AT $t = 10.60$, BASELINE CASE

Two vortices, V_1 and V_2, shed alternatively from the suction side and the pressure side of the airfoil, respectively. The vorticity field in Figure 7 shows that vortices that shed from the suction side rotate in clockwise direction while the vortices that shed from the pressure, caused by the pressure of the vortices from the suction side, side rotate in counterclockwise direction.

The time series of the lift and the drag coefficient in Figure 8 show an oscillating trend that is associated with the periodic pressure changes induced by the periodic vortex shedding. The average value of lift and drag is $c_l = 0.4465$ and $c_d = 0.0504$, respectively.

According to Haller's theory[9] the Lagrangian separation point is fixed for a periodic flow and is located

at the location of time-averaged zero skin friction friction. From the plot of the time-averaged skin friction coefficient versus distance in Figure 9, it is found that the Lagrangian flow separation is at $x/c = 0.5$.

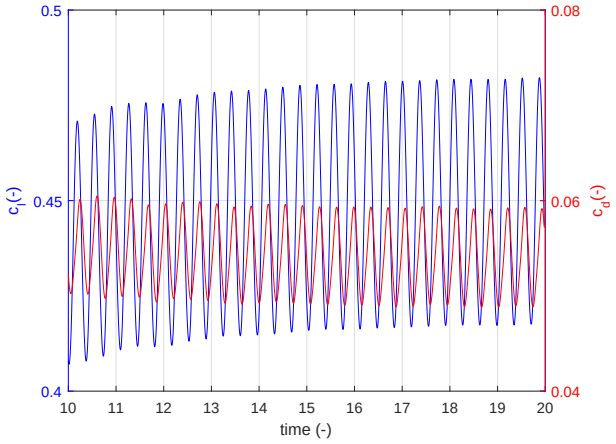

Figure 8. NACA 65(1)-412, $\alpha = 4°$, $Re_c = 20,000$, TIME SERIES OF THE LIFT AND DRAG COEFFICIENTS FOR THE BASELINE (NO PULSE ACTUATION)

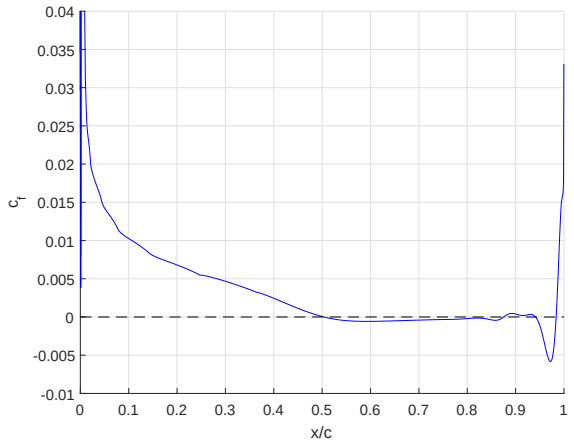

Figure 9. TIME-AVERAGED SKIN FRICTION COEFFICIENT ALONG THE SUCTION SIDE ON THE TIME INTERVAL $t = [10, 20]$

To visualize the separated material line, the maximum FTLE ridge is extracted from the FTLE field. This line is plotted in Figure 10 together with a linear approximation of the separation manifold described above. These two lines intersect and form the separatrix (separator of fluid) for this flow. To the best of our knowledge this connection between a separation manifold and the LCS field has not been visualized before. Because of the periodic shedding and feedback, the separation angle oscillates around an equilibrium value of $\theta = 7.77°$ with respect to the airfoil surface and has an amplitude of oscillation of $0.22°$.

Pulse actuation analysis

While a pulse placed downstream of the separation point does not effect the flow much, the effects of a pulse placed inside the boundary layer upstream of the separation point are significant. Moreover, they are qualitatively very similar for any pulse location P.

The pulse induces a flow perturbation (Fig. 11a) that is transported along the top of the shear layer. The perturbation grows as it travels downstream (Fig. 11a-d) inducing a Kelvin-Helmholtz like instability (Fig. 11b). A vortex pair forms on the suction side of the airfoil (Fig. 11c). While one of these vortices, V_4, sheds quickly (Figs. 11c and d), the second vortex, V_3, resides in the circulation region and grows in size.

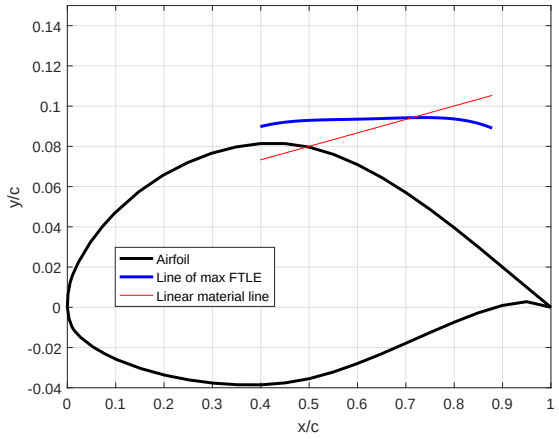

Figure 10. NACA 65(1)-412, $\alpha = 4°$, $Re_c = 20,000$, APPROXIMATE SEPARATION PROFILE AT $t = 11.00$ FOR THE BASELINE CASE (NO PULSE ACTUATION)

Coinciding with the shedding of the first vortex, the separated LCS wraps around vortex V_3 in Figures 11c and d) and aligns with the airfoil surface. This corresponds to a downward deflection of the separated shear layer towards the airfoil surface. and a reduction of the size of the recirculation area. This in turn yields a decrease in the pressure drag. Vortex V_4 also increases the vorticity in the recirculation area, as observed from the vorticity in Figure 16a. This leads to an increase in the lift.

Just like the backward-time LCS identifies flow separation, the intersection of an unstable material line in the forward-time LCS field with the airfoil surface identifies flow reattachment.[9] By comparing Figures 12 (with pulse actuation) and 13 (without pulse actuation), we observe a reattaching material line in the repelling FTLE field.

The time series of the lift and the drag coefficient for all cases are shown in Figure 14 and Figure 15, respectively. The drag coefficient decreases as the size of the recirculation area shrinks (compare Figs. 11c and d, and Fig. 15). The increase in lift coincides with the development of the large vortex, V_4, along the suction side. The maximum in the lift coefficient that is observed in Figure 14 coincides with a maximum strength of the vortex V_4 (Fig. 16a). At that time, the instantaneous pressure difference between the pressure side and the suction side is the largest (Fig. 17).

When the large vortex sheds, the lift coefficient decreases and is at that point lower than the lift coefficient of the baseline configuration. The drag coefficient on the other hand increases and is larger than that of the baseline case. A series of smaller vortices denoted by V_5 in Figures 16a-c, develop in the aftermath of the shedding, but appear to have only a small effect on the lift and the drag.

Because of feedback of the wake, the cycle of vortex development and shedding is repeated a number of times but with decreasing impact on lift and drag until the quasi-steady state baseline result is recovered. This cycle repetition can be very clearly seen for a pulse control at $x/c = 0.4$ and $x/c = 0.5$ and is weaker for the other pulse control locations.

The effects of the pulse on the shear layer and the recirculation area is the largest for the pulse located closest to, but upstream of the separation point $x/c = 0.5$. If the pulse is placed exactly at the separation point, a maximum increase in the lift coefficientis observed of roughly 40% with respect to the baseline as seen in Figure 14. The results obtained with pulse actuation between $x/c = 0.2$ and $x/c = 0.5$ are very similar in terms of the effects that were observed on the recirculation area and the LCSs. The time series of the lift and drag coefficient are also similar but have shifted in time with respect to each other because the changed advection time of the perturbation for different pulse locations. The closer the pulse is placed to the separation point, the earlier the peak in the lift coefficient is observed.

A time sequence of the approximation for the separation line is shown in Fig. 18. As the angle of the material line with the airfoil surface decreases, the line of maximum FTLE moves away from the airfoil surface. The line of maximum FTLE moves towards the airfoil surface with increasing angle of separation. The change in angle of the material line leads to changes in the concavity of the line. A decrease in the angle of the material line leads to a convex material line, while an increase in the angle of the material line

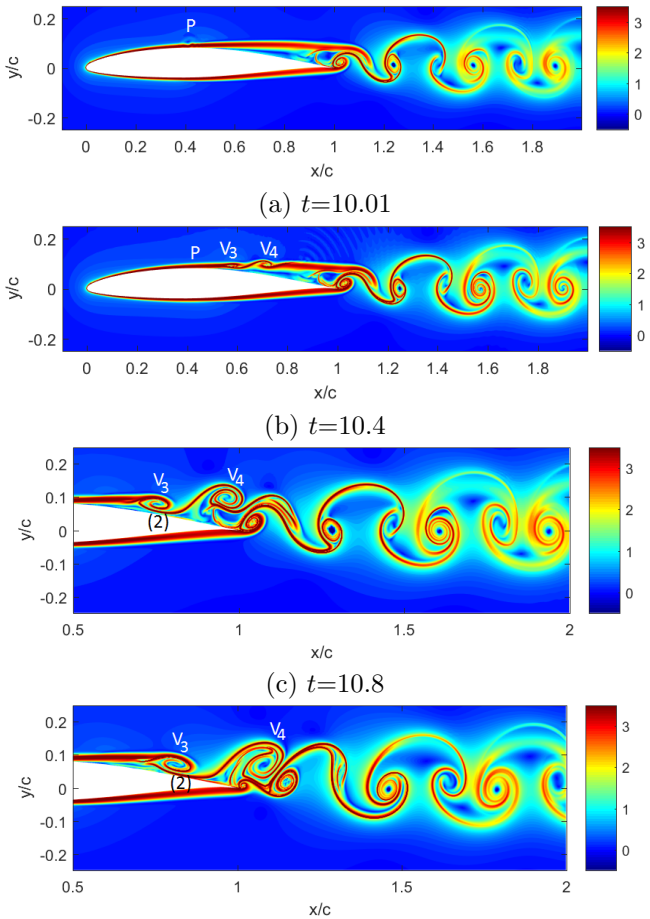

(a) t=10.01

(b) t=10.4

(c) t=10.8

(d) t=11.0

Figure 11. NACA 65(1)-412, $\alpha = 4°$, $Re_c = 20,000$, BACKWARD-TIME FTLE FIELD NEAR THE WAKE AT (a) t=10.01, (b) t=10.4, (c) t=10.8, and (d) t=11.0 FOR THE CASE WITH A PULSE ACTUATION AT $x/c = 0.4$

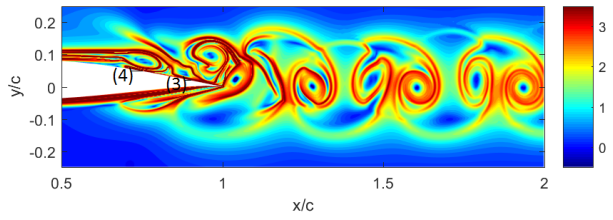

Figure 12. NACA 65(1)-412, $\alpha = 4°$, $Re_c = 20,000$, FORWARD-TIME FTLE FIELD AT $t = 10.80$ FOR THE CASE WITH A PULSE ACTUATION AT $x/c = 0.4$

leads to a concave FTLE line, moving the separation line closer to the airfoil surface and thus yielding a flow reattachment.

CONCLUSIONs AND RECOMMENDATIONS

The effect of pulse actuation on the unsteady separated Lagrangian flow over a NACA 65(1)-412 airfoil has been investigated.

Because of the pulse actuation, vortex structures develop along the suction side. The vortices induce a

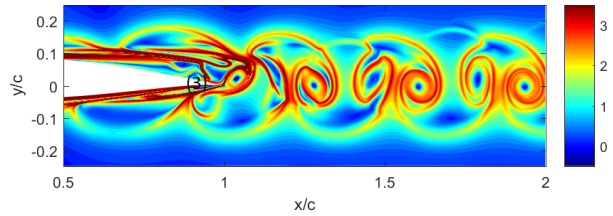

Figure 13. NACA 65(1)-412, $\alpha = 4°$, $Re_c = 20,000$, FORWARD-TIME FTLE FIELD AT $t = 10.80$ FOR THE BASELINE CASE (NO PULSE ACTUATION)

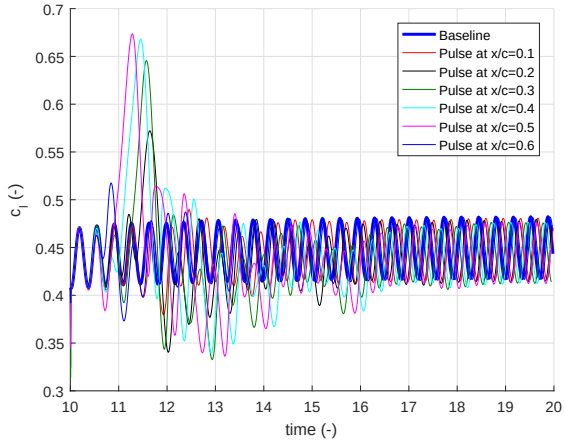

Figure 14. NACA 65(1)-412, $\alpha = 4°$, $Re_c = 20,000$, TIME SERIES OF THE LIFT COEFFICIENT FOR THE BASELINE AND SIX CASES WITH PULSE ACTUATION

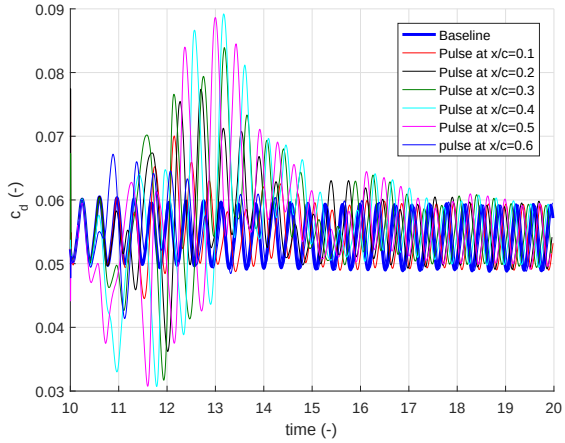

Figure 15. NACA 65(1)-412, $\alpha = 4°$, $Re_c = 20,000$, TIME SERIES OF THE DRAG COEFFICIENT FOR THE BASELINE AND SIX CASES WITH PULSE ACTUATION

flow reattachment that leads to a decrease in the pressure drag. An accompanying increase in vorticity leads to an increase in the instantaneous lift coefficient. The largest effect of the pulse is obtained when the pulse is placed close to and upstream of the separation point. The instantaneous lift coefficient can increase up to 40% compared to the baseline because of the effects of the pulse. The further the pulse is placed upstream, the smaller the impact of the pulse on the lift and drag coefficients.

Lagrangian analysis connected the unsteady behavior of the near wall separation lines and the connected development of Lagrangian Coherent Structures. An increased separation angle leads to reattachment be-

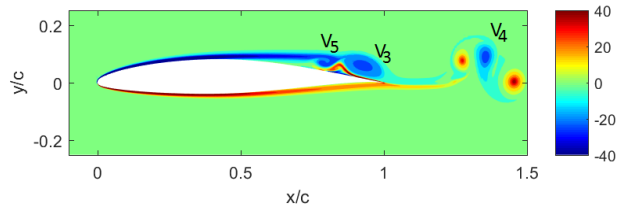

(a) t=11.4

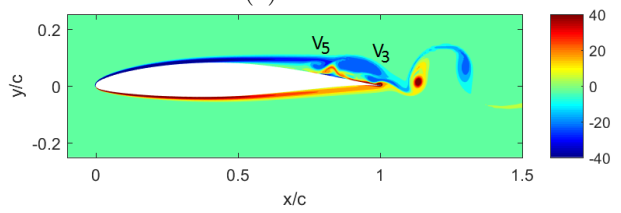

(b) t=12.0

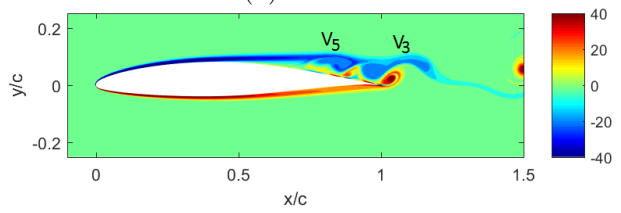

(c) t=12.4

Figure 16. NACA 65(1)-412, $\alpha = 4°$, $Re_c = 20,000$, VORTICITY FIELD AT (a) t=11.4, (b) t=12.0 and (c) t=12.4 FOR THE CASE WITH A PULSE ACTUATION AT $x/c = 0.4$

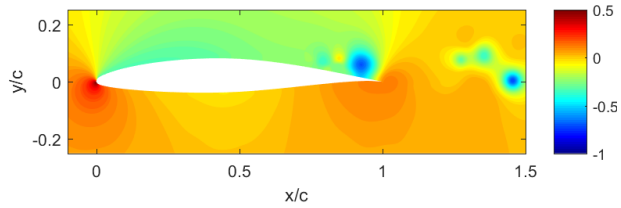

Figure 17. NACA 65(1)-412, $\alpha = 4°$, $Re_c = 20,000$, PRESSURE FIELD AT $t = 11.40$ FOR THE CASE WITH A PULSE ACTUATION AT $x/c = 0.4$

cause of concavity of the separation line, while a decreased separation angle increases the separation region because the material line is convex.

The results obtained for the impulse response serve as a starting point for the development of a complete theoretical framework for an active feedback flow control, which is part of ongoing research.

ACKNOWLEDGEMENT

We gratefully acknowledge funding under AFOSR-G00011458 of the Flow Control Program headed by Douglas Smith and funding from Solar Turbines.

References

[1]Schlichting, H. and Gersten, K., *Boundary-Layer Theory*, Springer-Verlag, New York, 1999.

[2]White, F. M., *Viscous Fluid Flow*, McGraw-Hill, New York, NY, 1991.

[3]Jeong, P. I., *Synthetic Jet Flow Control of Two-Dimensional NACA 65(1)-412 Airfoil Flow with Finite-Time Lyapunov Exponent Analysis of Lagrangian Coherent Structures*, Master thesis, San Diego State University, San Diego, CA, Summer 2016.

[4]Al-Arabi, M., "Experimental Investigation of the use of Synthetic Jets for Mixing in Vessels," *Journal of Fluids Engi-*

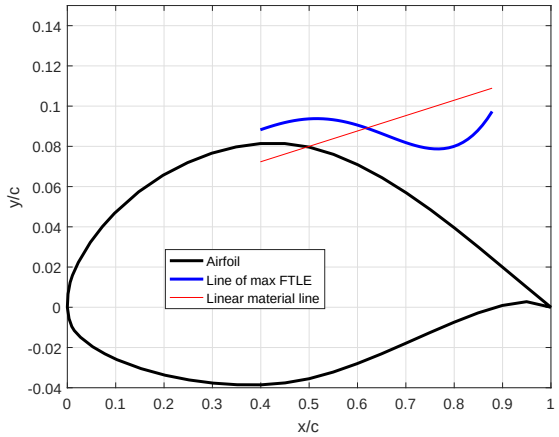

(a) t=11.0

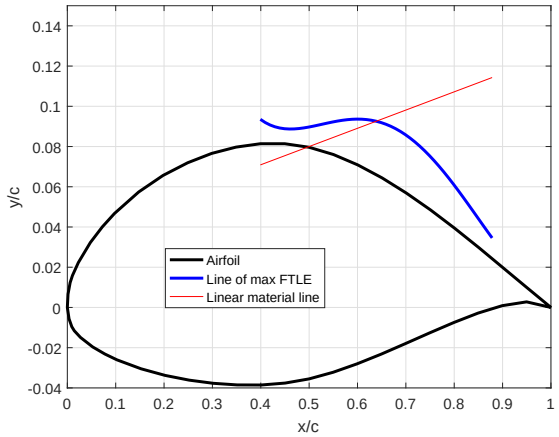

(b) t=11.4

Figure 18. NACA 65(1)-412, $\alpha = 4°$, $Re_c = 20,000$, APPROXIMATE SEPARATION PROFILE AT (a) t=11.0 and (b) $t = 11.40$ FOR THE CASE OF A PULSE ACTUATION AT $x/c = 0.4$

neering, Vol. 133, No. 9, September 12 2011, pp. 1–4.

[5]Post., M. L., *Plasma Actuators for Separation Control on Stationary and Oscillating Airfoils*, PhD Thesis, University of Notre Dame, Notre Dame, Indiana, May 2004.

[6]Acikel, H. H. and Genc, M. S., "Flow Control with Perpendicular Acoustic Forcing on NACA 2415 Aerfoil at Low Reynolds Numbers," *Journal of Aerospace Engineering*, Vol. 230, No. 13, December 12 2016, pp. 2447–2462.

[7]Torres, R. B., *Experimental Study of the use of Synthetic Jet Actuators for Flight Control*, Master thesis, San Diego State University, San Diego, CA, Fall 2014.

[8]Chen, K. K. and Rowley, C. W., "H_2 optimal actuator and sensor placement in the linearised complex Ginzburg–Landau system," *Journal of Fluid Mechanics*, Vol. 681, August 2011, pp. 241–260.

[9]Haller, G., "Exact Theory of Unsteady Separation for Two-Dimensional Flows," *Journal of Fluids Mechanics*, Vol. 512, March 26 2004, pp. 257–311.

[10]Haller, G., "Lagrangian Coherent Structures," *Annual Review of Fluid Mechanics*, Vol. 47, August 28 2014, pp. 137–162.

[11]Chen, K. K. and Rowley, C. W., "Heuristics for Effective Actuator and Sensor Placement in Feedback Flow Control," *Active Flow and Combustion Control*, edited by R. King, Vol. 127 of *Notes on Numerical Fluid Mechanics and Multidisciplinary Design*, Springer International Publishing Switzerland, 2014, pp. 115–130.

[12]Nelson, D. A., Jacobs, G. B., and Kopriva, D. A., "Effect of Boundary Representation on Viscous, Separated Flows in a Discontinuous-Galerkin Navier-Stokes Solver," *Theoretical Computational Fluid Dynamics*, Vol. 30, March 30 2016, pp. 363–385.

[13]Nelson, D. A. and Jacobs, G. B., "DG-FTLE: Lagrangian coherent structures with high-order discontinuous-Galerkin methods," *J. Comp. Phys.*, Vol. 295, 2015, pp. 65–86.

[14]Mohseni, K., Lipinski, D., and Cardwell, B., "A Lagrangian Analysis of a Two-Dimensional Airfoil with Vortex Shedding," *Journal of Physics A: Mathematical and Theoretical*, Vol. 41, No. 34, August 11 2008, pp. 1–22.

[15]Suzuki, T., Colonius, T., and Pirozzoli, S., "Vortex Shedding in a Two-Dimensional Diffuser: Theory and Simulation of Separation Control by Periodic Mass Injection," *Journal of Fluid Mech.*, Vol. 520, August 4 2004, pp. 187–213.

[16]Pasquetti, R. and Peres, N., "A Penalty Model of Synthetic Micro-Jet Actuator with Application to the Control of Wake Flows," *Elsevier, Computers and Fluids*, Vol. 114, March 7 2015, pp. 203–217.